Thermal-Mechanical Analysis of a Power Module with Parametric Model Order Reduction

Sheikh Hassan[1,*], Pushparajah Rajaguru[1], Stoyan Stoyanov[1], Christopher Bailey[2]
[1]*School of Computing and Mathematical Sciences, University of Greenwich, London, United Kingdom.*
[2]*School of Electrical, Computer and Energy Engineering, Arizona State University, Arizona, United States.*
[*]*Corresponding Author: s.r.hassan@greenwich.ac.uk.*

***Abstract*—This paper presents parametric model order reduction (pMOR) by the Lagrange approach of matrix interpolation for the thermal-mechanical and reliability study of a power electronics module (PEM) with nonlinear behaviours. Most previous research in model order reduction (MOR) studies reports thermal-mechanical simulations using a sequentially coupled method. In this research, a direct-coupled thermal-mechanical analysis, which simultaneously solves the thermal and structural governing equations, has been used to obtain thermal and deformation results. Furthermore, for pMOR, the linear approach of matrix interpolation is limited to linear changes between sampled-parametric points. Hence, a new way of interpolating system matrices using the Lagrange interpolation method has been adopted to implement the matrix interpolation efficiently. The parametric reduced-order model (pROM) solution by the Lagrange approach of matrix interpolation agrees well with the full-order model (FOM) and takes similar computational time as the linear (bi-linear) approach of matrix interpolation. pROM simulations offer up to 85.5% reduction in computational time.**

***Index Terms*—Finite Element Method, Thermal-Mechanical Analysis, Power Electronics Module, Reliability Assessment, Parametric Model Order Reduction.**

I. Introduction

New advanced technologies in industries, e.g., space & defence, energy, renewable energies and transportation, introduce complex and expensive projects to engineers and scientists. Reliability analysis is one of the most crucial factors of these technologies in keeping them safe and operational. Luckily, mathematical models can simulate the physical behaviours of domains and provide in-depth data for analyses and designs. Engineering sciences and their derived PDEs (partial differential equations) are capable of successfully describing physical behaviours of systems. One of the most widely used computational methods to solve PDEs is FEM/FEA (finite element method/analysis). For FEM computation, PDEs are discretised to algebraic equations via approximate unknown variables, which have complex and notably high dimensional systems of differential equations [1]. FEM provides excellent prediction, but in terms of simulating large-scale models or design points explorations, the computational time requirement is challenging, which is why model order reduction (MOR) is vital. In present literature, Krylov subspace-based MOR methods have been commonly used as they are "semi-automatic" compared to the Modal truncation method, a classic reduced order modelling method [2, 3].

Thermal behaviours of electric systems can cause performance degradation and reliability issues. Thermoelastic damping is one of the critical causes of these systems' component deterioration. Therefore, reliability assessment based on thermal-mechanical analysis is a crucial subject of study. Previously, Eblen [4] carried out a coupled thermomechanical analysis-based reliability study of electronics components with the help of FEM and CARES, a computing tool for reliability assessments. Thermomechanical analysis of an electronic package was presented by Codecasa et al. [5], focusing on reducing computing time with TRIC, a projection-based solver. Coupled thermomechanical analysis has been extended to electrical-thermal-mechanical analysis to study an electrical contact site by Shen and Ke [6].

Thermal analysis with MOR techniques is also helpful in reducing computing time for reliability assessments. Krylov subspace-based MOR techniques have been utilised for thermal analysis of an electric converter assembly by Liu et al. [7]. Thermal boundary condition independency of Krylov subspace-based reduced order modelling approach has been examined for thermal and coupled thermal analysis by Rogié et al. [8] and Codecasa et al. [9, 10].

Reduced order modelling for coupled problems is highly desirable due to the complexity of systems. Choi et al. [11] used Krylov subspace-based MOR technique to achieve a coupled thermal-mechanical ROM (reduced order model) of a micro-resonator. Rajaguru et al. [12] examined electrical loading in a PEM structure using ROMs built with Krylov subspace-based MOR techniques. A coupled electrical-thermal-mechanical model of a MEMS microgripper was studied by Binion and Chen [13], exploring several MOR techniques.

Parametric modelling is crucial for design point explorations and optimisations, and the parametric reduced order model (pROM) presents an appropriate solution to overcome computational time requirement issues that arise during parametric modelling. Bissuel et al. [14] surveyed numerous thermal models of electronic boards to optimise the device by building pROM based on the modal approach of MOR. Baur et al. [15] demonstrated parameterisation of the physical properties of a micro-thruster through various pMOR (parametric model order reduction) approaches in its frequency response investigation. Feng et al. [16] have developed electrical and coupled electrothermal pROMs to enhance the geometric

parameters of a nanoelectronics structure. A superposition principle-based pMOR approach has been used by ter Maten et al. [17] to change several variables of coupled electromagnetic-thermal models of electronic devices. Bouhedma et al. [18] built a Krylov subspace-based pROM for a piezoelectric energy harvester to modify the physical dimensions of the model. Schütz et al. [19] looked at several ROMs of a micro-actuator to transform its magnetostatic variables. An optimised model of a miniaturised thermoelectric generator has been created by Yuan et al. [20] exercising multiple pMOR methodologies.

Considering nonlinear behaviours in a model is a central part of an analysis as it provides in-depth data, and building a nonlinear ROM is advantageous as nonlinear computation requires relatively more time. Scognamillo et al. [21] exercised a MOR code, FANTASTIC, to evaluate the nonlinear thermal activities of a coupled electrothermal PEM model. A multi-physical ROM of a piezoelectric actuator considering nonlinear inputs was achieved, through Krylov subspace-based MOR method, by Schütz et al. [22]. In a recent investigation [23], the temperature-dependent coefficient of thermal expansion (CTE) of the wire material of a PEM has been parametrised in direct coupled thermal-mechanical parametric reduced order modelling.

The sequential coupling method has been widely exercised in most afore-mentioned studies for thermal-mechanical ROMs. Direct coupled thermal-mechanical analyses offer more sensible and precise insights into systems and should be considered in reduced-order modelling. The direct coupling method, which concurrently solves thermal and structural equations, has been utilised in this work for the thermo-mechanical ROM. Temperature-dependent material properties have been varied here for design point exploration, as prior pMOR studies only focused on changing constant model parameters. Nonlinear plasticity behaviour is also evaluated for the wire material of the PEM structure. The matrix interpolation method has been expanded to a new way of interpolating matrices, based on Lagrange interpolation, to create the pROM with a Krylov subspace-based pMOR approach for the current analysis.

II. Problem Formulation

A. Parametric Full Order Model (pFOM)

The state-space representation of the parametric full-order model (pFOM) is stated as the followings [20, 24]:

$$\begin{aligned} \boldsymbol{E}(\boldsymbol{p}_i)\dot{\boldsymbol{x}}(\boldsymbol{p}_i,t) &= \boldsymbol{A}(\boldsymbol{p}_i)\boldsymbol{x}(\boldsymbol{p}_i,t) + \boldsymbol{B}(\boldsymbol{p}_i)\boldsymbol{u}(\boldsymbol{p}_i,t) \\ \boldsymbol{y}(\boldsymbol{p}_i,t) &= \boldsymbol{C}(\boldsymbol{p}_i)\boldsymbol{x}(\boldsymbol{p}_i,t) \end{aligned} \tag{1}$$

$\boldsymbol{E}(\boldsymbol{p}_i), \boldsymbol{A}(\boldsymbol{p}_i) \in \mathbb{R}^{N\times N}$ are parametric point ($\boldsymbol{p}_i$) dependent system matrices, with $\boldsymbol{B}(\boldsymbol{p}_i) \in \mathbb{R}^{N\times M}$ and $\boldsymbol{C}(\boldsymbol{p}_i) \in \mathbb{R}^{P\times N}$ representing input and output matrices. $\boldsymbol{u}(\boldsymbol{p}_i,t) \in \mathbb{R}^M$ and $\boldsymbol{y}(\boldsymbol{p}_i,t) \in \mathbb{P}$ are parametric point ($\boldsymbol{p}_i$) and time (t) dependent inputs and outputs of the model together with $\boldsymbol{x}(\boldsymbol{p_i},t) \in \mathbb{N}$, which defines the states. $\boldsymbol{p}_i$ is the vector of model parametric points for design point explorations with $i = 0, 1, \ldots k$, and k identifies the total parametric points.

B. Projection-based Model Order Reduction (MOR)

The state-space representation of the full-order model (FOM), which is the non-parametric-point-dependent form of the model shown in (1), is stated as the followings [20, 24]:

$$\begin{aligned} \boldsymbol{E}\dot{\boldsymbol{x}}(t) &= \boldsymbol{A}\boldsymbol{x}(t) + \boldsymbol{B}\boldsymbol{u}(t) \\ \boldsymbol{y}(t) &= \boldsymbol{C}\boldsymbol{x}(t) \end{aligned} \tag{2}$$

$\boldsymbol{E}, \boldsymbol{A} \in \mathbb{R}^{N\times N}$ are system matrices, with $\boldsymbol{B} \in \mathbb{R}^{N\times M}$ and $\boldsymbol{C} \in \mathbb{R}^{P\times N}$ representing input and output matrices, they are parametric point ($\boldsymbol{p}_i$) independent. $\boldsymbol{u}(\boldsymbol{p}_i,t) \in \mathbb{R}^M$ and $\boldsymbol{y}(\boldsymbol{p}_i,t) \in \mathbb{P}$ are only time (t) dependent inputs and outputs of the model together with $\boldsymbol{x} \in \mathbb{R}^N$, which defines the states. The order of the model, $N \in \mathbb{N}$, is significantly high.

The reduced order model (ROM) of the system expressed in (2) can be specified as follows [20, 24]:

$$\begin{aligned} \boldsymbol{E}_r\dot{\boldsymbol{x}}_r(t) &= \boldsymbol{A}_r\boldsymbol{x}_r(t) + \boldsymbol{B}_r\boldsymbol{u}_r(t) \\ \boldsymbol{y}_r(t) &= \boldsymbol{C}_r\boldsymbol{x}_r(t) \end{aligned} \tag{3}$$

The matrices in the reduced model, established in (3), are obtained by the following operations: $\boldsymbol{E}_r = \boldsymbol{V}^T\boldsymbol{E}\boldsymbol{V}$, $\boldsymbol{A}_r = \boldsymbol{V}^T\boldsymbol{A}\boldsymbol{V}$, $\boldsymbol{B}_r = \boldsymbol{V}^T\boldsymbol{B}$ and $\boldsymbol{C}_r = \boldsymbol{C}\boldsymbol{V}$, utilising PRIMA [25, 26], a Krylov subspace-based MOR procedure. $\boldsymbol{E}_r, \boldsymbol{A}_r \in \mathbb{R}^{q\times q}$, $\boldsymbol{B} \in \mathbb{R}^{q\times m}$, and $\boldsymbol{C} \in \mathbb{R}^{p\times q}$ have incredibly lower dimensions, $q \ll N$, as they are transformed via the projection matrix $\boldsymbol{V} \in \mathbb{R}^{N\times q}$. The transfer function of the FOM in (2) is used to obtain the projection matrix ($\boldsymbol{V}$), and then the transfer function of the ROM in (3) is determined. The full-order and reduced-order models' transfer functions are expressed as the followings [25, 26]:

$$\boldsymbol{Y}(s) = \boldsymbol{C}(s\boldsymbol{E} - \boldsymbol{A})^{-1}\boldsymbol{B} \tag{4}$$

$$\boldsymbol{Y}_r(s) = \boldsymbol{C}_r(s\boldsymbol{E}_r - \boldsymbol{A}_r)^{-1}\boldsymbol{B}_r \tag{5}$$

C. Interpolation of Sparse Matrices

Linear matrix interpolation of the system's sparse matrices in (2), described by $\boldsymbol{X} = \boldsymbol{E}, \boldsymbol{A}, \boldsymbol{B}$, can be utilised to construct a state-space system in (1) as the following [24, 27]:

$$\boldsymbol{X}(\boldsymbol{p}_i) = \boldsymbol{X}(\boldsymbol{p}_0) + \omega(\boldsymbol{p}_i)\,[\boldsymbol{X}(\boldsymbol{p}_k) - \boldsymbol{X}(\boldsymbol{p}_0)] \tag{6}$$

The values of weighting functions, $\omega(\boldsymbol{p}_i)$, are determined through the linear interpolation method. The bi-linear (or multilinear) approach, capable of sampling more than two parametric points, has been exercised previously for a study to implement matrix interpolation [23]. For this study, $i = 0, 1, ..., k$, where $k = 6$. The implemented bi-linear matrix interpolation method can be expressed as the followings [23]:

$$\begin{aligned} \boldsymbol{X}(\boldsymbol{p}_{i=0,1,2,3}) &= \boldsymbol{X}(\boldsymbol{p}_0) + \omega(\boldsymbol{p}_i)\left[\boldsymbol{X}(\boldsymbol{p}_{\frac{k}{2}}) - \boldsymbol{X}(\boldsymbol{p}_0)\right] \\ \boldsymbol{X}(\boldsymbol{p}_{i=4,5,6}) &= \boldsymbol{X}(\boldsymbol{p}_{\frac{k}{2}}) + \omega(\boldsymbol{p}_i)\left[\boldsymbol{X}(\boldsymbol{p}_k) - \boldsymbol{X}(\boldsymbol{p}_{\frac{k}{2}})\right] \end{aligned} \tag{7}$$

A new way of matrix interpolation, based on the Lagrange method, has been applied then as the following:

$$\boldsymbol{X}(\boldsymbol{p}_i) = \omega_0(\boldsymbol{p}_i)\boldsymbol{X}(\boldsymbol{p}_0) + \omega_{\frac{k}{2}}(\boldsymbol{p}_i)\boldsymbol{X}(\boldsymbol{p}_{\frac{k}{2}}) + \omega_k\boldsymbol{X}(\boldsymbol{p}_k) \tag{8}$$

D. Parametric Reduced Order Model (pROM)

The interpolated matrices illustrated in (7) and (8) and the MOR method outlined in (3) have been utilised to create pROMs. The pROM can be written as the followings [20]:

$$\begin{aligned} \boldsymbol{E}_r(\boldsymbol{p}_i)\dot{\boldsymbol{x}}_r(\boldsymbol{p}_i,t) &= \boldsymbol{A}_r(\boldsymbol{p}_i)\boldsymbol{x}_r(\boldsymbol{p}_i,t) + \boldsymbol{B}_r(\boldsymbol{p}_i)\boldsymbol{u}_r(\boldsymbol{p}_i,t) \\ \boldsymbol{y}_r(\boldsymbol{p}_i,t) &= \boldsymbol{C}_r(\boldsymbol{p}_i)\boldsymbol{x}_r(\boldsymbol{p}_i,t) \end{aligned} \tag{9}$$

The pROM in (9) has been solved by the generalized trapezoidal rule (GTR) [28, 29].

E. Parametric Thermal-Mechanical Model

The coupled thermal-mechanical model considered for this analysis is a second-order system; this is attained using FEM discretisation. The parametric-point-dependent discretised thermal-mechanical model is stated in the following forms [29, 30]:

$$\begin{aligned} \boldsymbol{M}(\boldsymbol{p}_i)\,\ddot{\boldsymbol{z}}(\boldsymbol{p}_i,t) + \boldsymbol{D}(\boldsymbol{p}_i)\dot{\boldsymbol{z}}(\boldsymbol{p}_i,t) + \boldsymbol{K}(\boldsymbol{p}_i)\boldsymbol{z}(\boldsymbol{p}_i,t) \\ = \boldsymbol{G}(\boldsymbol{p}_i)\boldsymbol{u}(\boldsymbol{p}_i,t) \\ \boldsymbol{y}(\boldsymbol{p}_i,t) = \boldsymbol{L}(\boldsymbol{p}_i)\boldsymbol{z}(\boldsymbol{p}_i,t) \end{aligned} \tag{10}$$

$\boldsymbol{M}(\boldsymbol{p}_i), \boldsymbol{D}(\boldsymbol{p}_i), \boldsymbol{K}(\boldsymbol{p}_i) \in \mathbb{R}^{n\times n}$ signify mass, damping and stiffness matrices, where $2n = N$, with $\boldsymbol{G}(\boldsymbol{p}_i) \in \mathbb{R}^{n\times M}$ and $\boldsymbol{L}(\boldsymbol{p}_i) \in \mathbb{R}^{P\times n}$ representing input and output matrices. $\boldsymbol{u}(\boldsymbol{p}_i,t) \in \mathbb{R}^{M}$ and $\boldsymbol{y}(\boldsymbol{p}_i,t) \in \mathbb{R}^{P}$ define the inputs and outputs of the model, with $\boldsymbol{z}(\boldsymbol{p}_i,t) \in \mathbb{R}^{n}$ depicting states. In general, matrices are described as the followings [29]:

$$\begin{aligned} &\boldsymbol{M} = \begin{bmatrix} \boldsymbol{M}_s & \boldsymbol{0} \\ \boldsymbol{0} & \boldsymbol{0} \end{bmatrix}, \boldsymbol{D} = \begin{bmatrix} \boldsymbol{D}_s & \boldsymbol{0} \\ \boldsymbol{D}^{tu} & \boldsymbol{D}^{t} \end{bmatrix}, \boldsymbol{K} = \begin{bmatrix} \boldsymbol{K}_s & \boldsymbol{K}^{ut} \\ \boldsymbol{0} & \boldsymbol{K}^{t} \end{bmatrix}, \\ &\boldsymbol{G} = \begin{bmatrix} \boldsymbol{F} \\ \boldsymbol{Q} \end{bmatrix}, \ddot{\boldsymbol{z}} = \begin{bmatrix} \ddot{\boldsymbol{z}}_{ut} \\ \ddot{\boldsymbol{T}} \end{bmatrix}, \dot{\boldsymbol{z}} = \begin{bmatrix} \dot{\boldsymbol{z}}_{ut} \\ \dot{\boldsymbol{T}} \end{bmatrix}, \boldsymbol{z} = \begin{bmatrix} \boldsymbol{z}_{ut} \\ \boldsymbol{T} \end{bmatrix} \end{aligned} \tag{11}$$

$$\text{with,} \quad \begin{aligned} &\boldsymbol{K}^t = \boldsymbol{K}^{tb} + \boldsymbol{K}^{tc}, \boldsymbol{F} = \boldsymbol{F}^{nd} + \boldsymbol{F}^{pr} + \boldsymbol{F}^{ac}, \\ &\boldsymbol{Q} = \boldsymbol{Q}^{nd} + \boldsymbol{Q}^{g} + \boldsymbol{Q}^{c} \end{aligned} \tag{12}$$

$\boldsymbol{M}_s$ denotes structural mass matrix. $\boldsymbol{D}_s$, $\boldsymbol{D}^{tu}$ and $\boldsymbol{D}^{t}$ correspond to structural and thermoelastic damping and thermal-specific heat matrices, respectively. $\boldsymbol{K}_s$, $\boldsymbol{K}^{tu}$ and $\boldsymbol{K}^{t}$ stand for structural and thermoelastic stiffness and thermal conductivity matrices, accordingly, while $\boldsymbol{K}^{tb}$ and $\boldsymbol{K}^{tc}$ indicate thermal conductivity matrices of material and convection surfaces. $\boldsymbol{F}$ signifies structural (mechanical) load vectors, with $\boldsymbol{F}^{nd}$, $\boldsymbol{F}^{pr}$ and $\boldsymbol{F}^{ac}$ describing nodal force and pressure load vectors and force vectors caused by acceleration effects correspondingly. $\boldsymbol{Q}$ represents the thermal load vector, whilst $\boldsymbol{Q}^{nd}$, $\boldsymbol{Q}^{c}$ and $\boldsymbol{Q}^{g}$ define nodal heat flow rate and convection surface vectors and heat generation rate vector without Joule heating, in that order. $\boldsymbol{z}_{ut}$ and $\boldsymbol{T}$ symbolise potential displacement and thermal vectors.

The state space model, presented in (1), can be formed by transforming the thermal-mechanical model, explained in (10), as the followings [30]:

$$\begin{aligned} &\begin{bmatrix} \boldsymbol{F} & \boldsymbol{0} \\ \boldsymbol{0} & \boldsymbol{M} \end{bmatrix} \begin{bmatrix} \dot{\boldsymbol{z}} \\ \ddot{\boldsymbol{z}} \end{bmatrix} = \begin{bmatrix} \boldsymbol{0} & \boldsymbol{F} \\ -\boldsymbol{K} & -\boldsymbol{D} \end{bmatrix} \begin{bmatrix} \boldsymbol{z} \\ \dot{\boldsymbol{z}} \end{bmatrix} + \begin{bmatrix} \boldsymbol{0} \\ \boldsymbol{G} \end{bmatrix} \boldsymbol{u} \\ &\boldsymbol{y} = \begin{bmatrix} \boldsymbol{L} & \boldsymbol{0} \end{bmatrix} \begin{bmatrix} \boldsymbol{z} \\ \dot{\boldsymbol{z}} \end{bmatrix} \end{aligned} \tag{13}$$

$$\text{with,} \quad \begin{aligned} &\boldsymbol{E} = \begin{bmatrix} \boldsymbol{F} & \boldsymbol{0} \\ \boldsymbol{0} & \boldsymbol{M} \end{bmatrix}, \boldsymbol{A} = \begin{bmatrix} \boldsymbol{0} & \boldsymbol{F} \\ -\boldsymbol{K} & -\boldsymbol{D} \end{bmatrix}, \boldsymbol{B} = \begin{bmatrix} \boldsymbol{0} \\ \boldsymbol{G} \end{bmatrix}, \\ &\boldsymbol{C} = \begin{bmatrix} \boldsymbol{L} & \boldsymbol{0} \end{bmatrix}, \dot{\boldsymbol{x}} = \begin{bmatrix} \dot{\boldsymbol{z}} \\ \ddot{\boldsymbol{z}} \end{bmatrix}, \boldsymbol{x} = \begin{bmatrix} \boldsymbol{z} \\ \dot{\boldsymbol{z}} \end{bmatrix} \end{aligned} \tag{14}$$

$\boldsymbol{F}$ has to be non-singular here. $\boldsymbol{F} = \boldsymbol{I}_n$ is assumed, for the presented system, with $\boldsymbol{I}_n$ as an $n \times n$ identity matrix.

III. Power Electronics Module (PEM)

For this analysis, we focused on a *2D*-plane model of a PEM to explore its thermal-mechanical behaviours for a set of parameteric points. This PEM has *SiC* as semiconductors. The physical dimensions of the PEM structure and boundary conditions set for the direct-coupled analysis are described in Fig. 1. For the model built in ANSYS, *Al* (alloy) has been assumed as the wire material, and the properties of this material will be parametrised in this pMOR study.

A. FEM Model

In the FEM model, a direct coupled transient thermal-mechanical analysis has been exercised for the present investigation. The *SiC* bodies of the model act as thermal sources and have an isothermal boundary condition with a maximum value of $T_{SiC} = 200°C$ (labelled A in Fig. 1). The bottom surface of the baseplate, made of *Cu* material, has a convection boundary condition with a maximum convection coefficient of $h = 5W/mm^2 \cdot^\circ C$ and a maximum ambient temperature of $T_C = 50°C$ (labelled C in Fig. 1) and reflects assumed ambient temperatures. The left and right corner vertices of the baseplate (*Cu*) are fixed with no anticipated deformation (labelled B in Fig. 1). The analysis has 11 loading steps as shown in Fig 2, and the heat-generating body and the convection surface have differing temperature and coefficient values throughout the simulation. Material properties data are retrieved from ANSYS booklet [31]. The wire material, *Al* (alloy), has nonlinear plasticity behaviour, which follows the nonlinear power hardening law. The power hardening law, based on Gurson's Model, is stated in the following [29, 32]:

$$\frac{\sigma_Y}{\sigma_0} = \left(\frac{\sigma_Y}{\sigma_0} + \frac{3G}{\sigma_0}\overline{\varepsilon}^p \right)^{N_S} \tag{15}$$

Here, σ_Y and σ_0 are current and initial yield strengths, and G is the shear modulus. $\overline{\varepsilon}^p$ represents the microscopic equivaent plastic strain, and N_S is the stress ratio. Initial yield stress ($280MPa$) and exponent (0.134) values for nonlinear plasticity modelling are assumed based on the approaches described in [29, 33].

B. Parametric Points

The thermal expansion coefficient, CTE_{Al}, and Young's Modulus, E_{Al}, of the *Al* (alloy) are temperature dependent. These properties of the material add further nonlinear behaviours to the body. CTE_{Al} and E_{Al} have been parametrised, for the current study, for design point exploration. Uniformly spaced parametric points have been preferred here to implement pMOR with matrix interpolation, as presented in Fig. 3. The parametric points have evenly spaced CTE_{Al} and E_{Al}

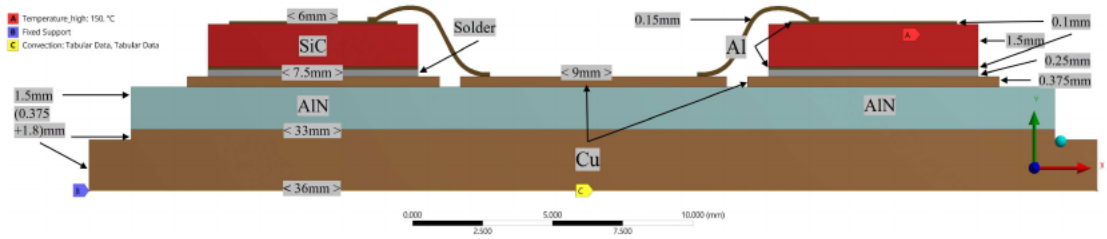

Fig. 1: *2D*-plane of the PEM structure and boundary conditions.

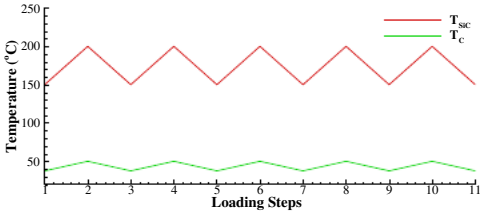

Fig. 2: Heat-generating body (T_{SiC}) and Ambient (T_C) temperatures during loading steps.

values corresponding to their temperature values. The ranges of CTE_{Al} and E_{Al} values considered for the parametric study are explained in Fig. 4 and Table I.

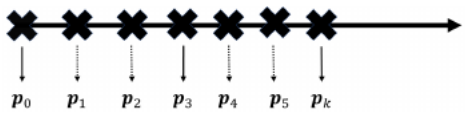

Fig. 3: Uniform parametric points.

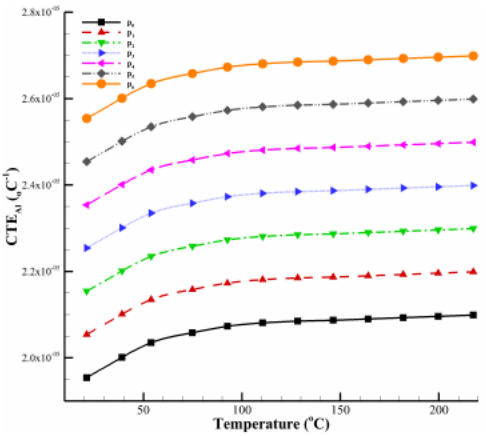

Fig. 4: Parametric points for the temperature dependent coefficient of thermal expansion of *Al* (alloy), CTE_{Al}.

C. Reduced Model

The total degrees of freedom (DOFs) of the state-space full-order model (FOM) is $N = 2n = 27,094$, with $N \times N$ system matrices. On the other hand, the reduced order model (ROM) has a total DOFs of $q = 8$, with $q \times q$ system matrices. This results in ROM demanding substantially less time for computation against its FOM. The overall simulation time

TABLE I: Parametric points for the temperature dependent Young's Modulus of *Al* (alloy), E_{Al}.

Parametric Points	**Young's Modulus (E_{Al}) in GPa**		
	$19.85\,^{\circ}C$	$116.3\,^{\circ}C$	$212.95\,^{\circ}C$
$\boldsymbol{p}_0$	71.06	70.12	69.18
$\boldsymbol{p}_1$	71.05	70.11	69.17
$\boldsymbol{p}_2$	71.04	70.10	69.16
$\boldsymbol{p}_3$	71.03	70.09	69.15
$\boldsymbol{p}_4$	71.02	70.08	69.14
$\boldsymbol{p}_5$	71.01	70.07	69.13
$\boldsymbol{p}_6$	71.00	70.06	69.12

in pROM, including order reductions of system matrices, is $608s$, which provides the solution for all seven parametric points. The pFOM-ANSYS solution, in comparison, would require around $4200s$ on the same computer. By means of the pMOR approach, a decline of 85.5% in computational time requirements has been accomplished.

Fig. 5 exhibits a flow chart summarising the stages of the pMOR study. The ANSYS Workbench/Mechanical has been used to create the PEM model, FEM discretisation and obtain the system matrices for three sampled-parametric points ($\boldsymbol{p}_0$, $\boldsymbol{p}_3$ and $\boldsymbol{p}_6$). System matrices are extracted as sparse matrices due to their compactness. The matrices have been then imported into MATLAB to develop the pROM with the pMOR method.

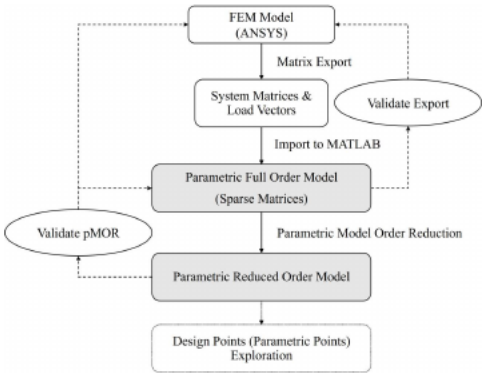

Fig. 5: The organizational process to build the pROM.

D. Results and Discussions

The pROM outcomes must align with the FOM-ANSYS solution to verify that the valid pROM has been built. The model's DOFs are temperature and directional deformations,

in this case, directional deformations in the x and y-axis. Fig. 6 illustrates the temperature and total deformation distributions for the left section of the PEM structure, assessing the results from FOM-ANSYS and pROM with Lagrange interpolation. In addition to the MOR approach, the means of matrix interpolation must be confirmed, so the interpolated point's ($\boldsymbol{p}_2$) solution from the pROM has been evaluated in this figure. The pROM solution demonstrates excellent agreement compared to the FOM-ANSYS solution.

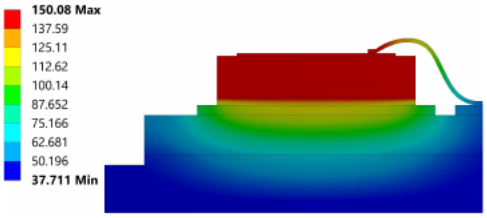

(a) Temperature ($^{\circ}C$), FOM-ANSYS solution.

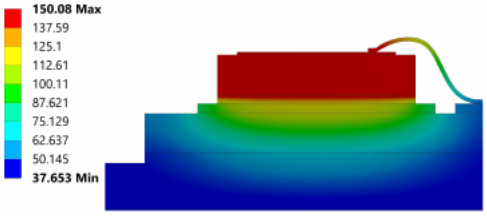

(b) Temperature($^{\circ}C$), pROM solution.

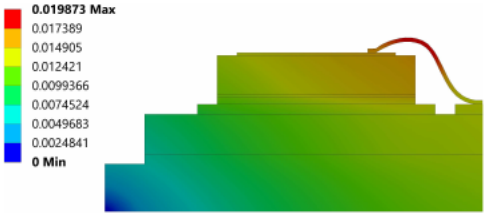

(c) Total deformation (mm), FOM-ANSYS solution.

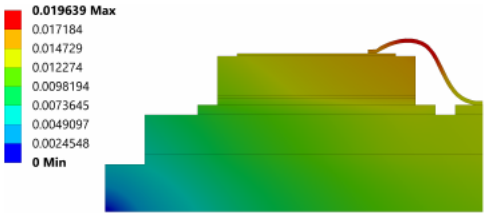

(d) Total deformation (mm), pROM solution.

Fig. 6: Temperature ($^{\circ}C$) and Total Deformation (mm) distribution from FOM-ANSYS and pROM (Lagrange) solutions in the left part of the PEM structure for the interpolated-parametric point $\boldsymbol{p}_2$.

The wire bond site experiences one of the highest temperatures, seen in Fig. 6a and 6b. The temperature here goes up to that of the heat-generating body, the *SiC*-based semiconductor. The *Min* temperature values for the PEM structure differ only by 0.15% between the FOM-ANSYS and pROM solutions, and there is no difference in the *Max* temperature. This wire bond site will be the focus of the presenting result analysis.

Figs. 6c and 6d indicate that the wire and wire bond site of the PEM structure undergo a significant amount of deformation. The FOM-ANSYS and pROM solutions vary by about 1.8% in terms of the total deformation peak value. The wire body was expected to show the peak deformation in the PEM model.

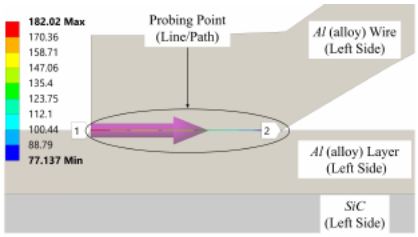

(a) Equivalent (von-Mises) stress (MPa), obtained by the FOM-ANSYS solution, along the probing point (line/path) in the PEM for interpolated-parametric point $\boldsymbol{p}_2$.

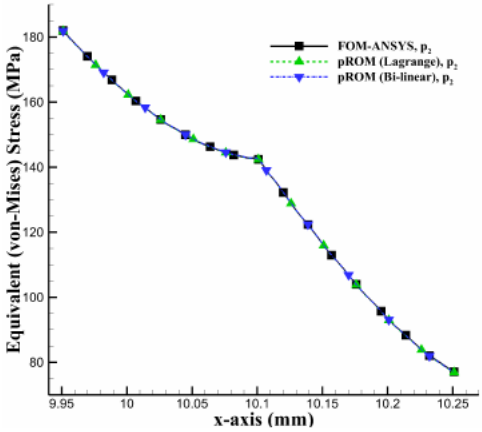

(b) Equivalent (von-Mises) stress, FOM-ANSYS vs pROM solution, for the interpolated-parametric point $\boldsymbol{p}_2$.

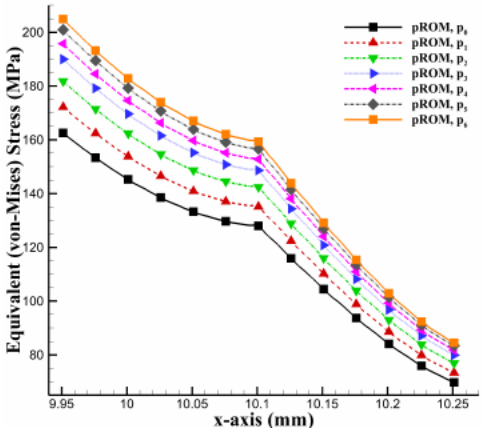

(c) Equivalent (von-Mises) stress, obtained by the pROM (Lagrange) solution, for all the parametric points.

Fig. 7: Maximum Equivalent (von-Mises) stress over time along a probing point in wire bond site (in wire body) of the PEM structure.

The maximum equivalent (von-Mises) stresses over time in the wire bond site (in wire body) are presented in Fig. 7. The depicted results are obtained from a probing point, which is a line/path along the wire bond shown in Fig. 7a, considering

the significance of the site [34]. FOM-ANSYS and pROM (Lagrange and Bi-linear) stress results are displayed in Fig. 7b for an interpolated-parametric point $\boldsymbol{p}_2$. Stress results obtained from the pROMs are in excellent agreement with the FOM-ANSYS result, with only a 0.1% average difference between the solutions. Thus, the pMOR approach is a suitable approximate modelling approach for reliability analysis-based design points exploration. Fig. 7c evaluates stress results obtained by the pROM (Lagrange) for all parametric points. *Max* stresses along the probing point extent from $181MPa$ to $206MPa$ for the studied parametric points, which is $< 280MPa$, the yield strength of the material. Non-zero equivalent plastic strain values are seen in this site at and after $\boldsymbol{p}_3$ and reach a maximum of $4.4 \times 10^{-4} mm/mm$ at $\boldsymbol{p}_6$ for current loading.

IV. Conclusion

The pMOR method has been exercised in this work to explore different parametric points of a directly coupled thermal-mechanical PEM model, considering nonlinear plasticity behaviours in the wire material. The temperature-dependent coefficient of thermal expansion and Young's modulus of the *Al* (alloy), the wire material, have been parametrised for the pROM. The MOR approach PRIMA has been utilised here to reduce computational time requirements. A new matrix interpolation technique, based on the Lagrange interpolation, which provides a better process of matrix interpolation for multiple sampled-parametric points compared to the linear/multilinear approach, has been offered here to build the pROM. The pROM requires 85.5% less computing time with only a 0.1% disparity vs FOM-ANSYS in stress results. The pMOR method can help reduce the time requirements of reliability analysis-based design explorations for large-scale models. Future studies will focus on applying this method to models with rate-dependent material nonlinearities.

References

[1] G. Dhatt, E. Lefrançois and G. Touzot, *Finite element method*, John Wiley & Sons, 2012.

[2] E. Davison, "A method for simplifying linear dynamic systems," IEEE Transactions on automatic control, vol. 11, no. 1, pp. 93-101, 1966.

[3] R. W. Freund, "Model reduction methods based on Krylov subspaces," Acta Numerica, vol. 12, pp. 267-319, 2003.

[4] M. Eblen, "Applied FEM techniques in ceramic feedthru package design," in 54th Electronic Components and Technology Conference (IEEE Cat. No. 04CH37546), 2004.

[5] L. Codecasa, *et al.*, "Towards the Extension of TRIC for Thermo-Mechanical Analysis," in 27th International Workshop on Thermal Investigations of ICs and Systems (THERMINIC), 2021.

[6] F. Shen and L. Ke, "Numerical study of coupled electrical-thermal-mechanical-wear behavior in electrical contacts.," Metals, vol. 11, no. 6, pp. 955, 2021.

[7] W. Liu, H. Torsten and J. Drobnik, "Effective Thermal Simulation of Power Electronics in Hybrid and Electric Vehicles," World Electric Vehicle Journal, vol. 5, no. 2, pp. 574-580, 2012.

[8] B. Rogié, *et al.*, "Multi-port dynamic compact thermal models of dual-chip package using model order reduction and metaheuristic optimization," Microelectronics Reliability, vol. 87, pp. 222-231, 2018.

[9] L. Codecasa, *et al.*, "Versatile MOR-based boundary condition independent compact thermal models with multiple heat sources," Microelectronics Reliability, vol. 87, pp. 194-205, 2018.

[10] L. Codecasa, V. d'Alessandro and D. D'Amore, "Altering MOR-based BCI CTMs into Delphi-like BCI CTMs," In 26th International Workshop on Thermal Investigations of ICs and Systems (THERMINIC), 2020.

[11] J. Choi, M. Cho and J. Rhim, "Efficient prediction of the quality factors of micromechanical resonators," Journal of Sound and Vibration, vol. 329, no. 1, pp. 84-95, 2010.

[12] P. Rajaguru, M. Bella and C. Bailey, "Applying Model Order Reduction to the Reliability Prediction of Power Electronic Module Wirebond Structure," in 27th International Workshop on Thermal Investigations of ICs and Systems (THERMINIC), 2021.

[13] D. Binion and X. Chen, "Coupled electrothermal-mechanical analysis for MEMS via model order reduction". Finite elements in analysis and design, vol. 46, no. 12, pp.1068-1076, 2010.

[14] V. Bissuel, *et al.*, "Multi-port Dynamic Compact Thermal Models of BGA package using Model Order Reduction and Metaheuristic Optimization.," in 18th IEEE Intersociety Conference on Thermal and Thermomechanical Phenomena in Electronic Systems (ITherm), 2019.

[15] U. Baur, *et al.*, "Comparison of methods for parametric model order reduction of instationary problems," Max Planck Institute for Dynamics of Complex Technical Systems, 2015.

[16] L. Feng, *et al.*, "Parametric modeling and model order reduction for (electro-) thermal analysis of nanoelectronic structures," Journal of Mathematics in Industry, vol. 6, no. 1, pp. 1-16, 2016.

[17] E. ter Maten, *et al.*, "Nanoelectronic COupled problems solutions-nanoCOPS: modelling, multirate, model order reduction, uncertainty quantification, fast fault simulation.," Journal of Mathematics in Industry, vol. 7, no. 1, pp. 1-19, 2016.

[18] S. Bouhedma, *et al.*, "System-level model and simulation of a frequency-tunable vibration energy harvester," Micromachines, vol. 11, no. 1, pp. 91, 2020.

[19] A. Schütz, *et al.*, "Parametric system-level models for position-control of novel electromagnetic free flight microactuator," Microelectronics Reliability, pp. 114062, 2021.

[20] C. Yuan, D. Hohlfeld and T. Bechtold, "Design optimization of a miniaturized thermoelectric generator via parametric model order reduction.," Microelectronics Reliability, vol. 119, pp. 114075, 2021.

[21] C. Scognamillo, *et al.*, "Compact Modeling of a 3.3 kV SiC MOSFET Power Module for Detailed Circuit-Level Electrothermal Simulations Including Parasitics," Energies, vol. 14, no. 15, pp. 4683, 2021.

[22] A. Schütz, S. Maeter and T. Bechtold, "System-Level Modelling and Simulation of a Multiphysical Kick and Catch Actuator System," Actuators, vol. 10, no. 11, pp. 279, 2021.

[23] S. Hassan, *et al.*, "Parametrising Temperature Dependent Properties in Thermal-Mechanical Analysis of Power Electronics Modules using Parametric Model Order Reduction", in 46th International Spring Seminar on Electronics Technology (ISSE), 2023.

[24] H. Panzer, *et al.*, "Parametric model order reduction by matrix interpolation," Automatisierungstechnik, vol. 58, no. 8, pp. 475-484, 2010.

[25] A. Odabasioglu, M. Celik and L. Pileggi, "PRIMA: Passive reduced-order interconnect macromodeling algorithm.", IEEE Transactions on computer-aided design of integrated circuits and systems, vol. 17, no. 8, pp. 645-654, 1998.

[26] S. Race, *et al.*, "Circuit-based electrothermal modeling of SiC power modules with nonlinear thermal models," IEEE Transactions on Power Electronics, vol. 37, no. 7, pp. 7965-7976, 2022.

[27] M. Geuss, H. Panzer and B. Lohmann, "On parametric model order reduction by matrix interpolation," in European Control Conference (ECC), 2013.

[28] T.J. Hughes, *The finite element method: linear static and dynamic finite element analysis*, Courier Corporation, 2012

[29] ANSYS, *Mechanical APDL 2023 R1 - Theory Reference*, ANSYS, 2023.

[30] B. Lohmann and B. Salimbahrami, "Reduction of second order systems using second order Krylov subspaces," in IFAC Proceedings Volumes, 2005.

[31] M. Ashby, *Material property data for engineering materials*, ANSYS, 2021

[32] A. L. Gurson, "Continuum theory of ductile rupture by void nucleation and growth: Part I—Yield criteria and flow rules for porous ductile media", Brown Univ., Providence, RI (USA). Div. of Engineering, 1977.

[33] T. Wierzbicki, *Structural Mechanics (Wierzbicki)*, Massachusetts Institute of Technology via MIT OpenCourseWare, 2023. [Online]. Available: https://eng.libretexts.org

[34] K. Nwanoro, *et al.*, "Advantages of the extended finite element method for the analysis of crack propagation in power modules," Power Electronic Devices and Components, vol. 4, pp. 100027, 2023.